PAPER • OPEN ACCESS

Study of broadband multimode light via non-phase-matched sum frequency generation

New Journal of Physics
The open access journal at the forefront of physics

Deutsche Physikalische Gesellschaft DPG
IOP Institute of Physics

Published in partnership with: Deutsche Physikalische Gesellschaft and the Institute of Physics

OPEN ACCESS

RECEIVED
5 October 2018

REVISED
10 February 2019

ACCEPTED FOR PUBLICATION
26 February 2019

PUBLISHED
28 March 2019

PAPER

Study of broadband multimode light via non-phase-matched sum frequency generation

Denis A Kopylov[1], **Kirill Yu Spasibko**[2,3,4], **Tatiana V Murzina**[1] **and Maria V Chekhova**[1,2,3]

[1] Department of Physics, M.V. Lomonosov Moscow State University, Leninskie Gory GSP-1, 119991 Moscow, Russia
[2] Max Planck Institute for the Science of Light, Staudtstr. 2, D-91058, Erlangen, Germany
[3] University of Erlangen-Nürnberg, Staudtstr. 7/B2, D-91058, Erlangen, Germany
[4] Author to whom any correspondence should be addressed.

E-mail: kopylov.denis@physics.msu.ru **and** kirill.spasibko@mpl.mpg.de

Keywords: high-gain parametric down-conversion, sum frequency generation, tight focusing, Schmidt modes, bright squeezed vacuum, quantum optics, nonlinear optics, non-phase-matched generation

Abstract

We propose non-phase-matched sum frequency generation (SFG) as a method for characterizing broadband multimode light. Both the central wavelength and the bandwidth are in this case not limited by the phase matching condition. As an example, we consider bright squeezed vacuum (BSV) generated through high-gain parametric down conversion (PDC). In the spectrum of SFG from BSV, we observe the coherent peak and the incoherent background. We show that the ratio of their widths is equal to the number of frequency modes in BSV, which in the case of low-gain PDC gives the degree of frequency entanglement for photon pairs. By generating the sum frequency in the near-surface region of a nonlinear crystal, we increase the SFG efficiency and get rid of the modulation caused by chromatic dispersion, known as Maker fringes. This allows one to use non-phasematched SFG as a wavelength-independent autocorrelator. Furthermore, we demonstrate efficient non-phase-matched three- and four-frequency summation of broadband multimode light, hardly possible under phase matching. We show that the latter contains the coherent peak while the former does not.

1. Introduction

Sum frequency generation (SFG) is one of the most convenient tools for the study of spectral and temporal structure of light. Time-domain SFG is the key part of different pulse characterization techniques such as autocorrelation [1], FROG [2] or SPIDER [3]. In particular, SFG is crucial for the study of nonclassical light as it can be used as a fast coincidence circuit to reveal entanglement between photons or photon-number correlations between bright twin beams [4–8].

For the SFG from broadband radiation, the well-known challenge is to make it efficient for the whole pump spectrum. The standard solution to increase the bandwidth of SFG is a thin phase matched nonlinear crystal or a quasi-phase-matched crystal with aperiodic poling. However, the bandwidth of such devices is still limited; moreover, in the case of quasi-phase-matching SFG strongly depends on the quality of the nonlinear lattice.

In this paper we propose to use non-phase-matched SFG in order to overcome the limitations set by phase matching. This way we drastically increase the frequency bandwidth and make the technique applicable to almost any bright input light. To compensate for the relatively low efficiency of non-phase-matched SFG, we use a crystal with high quadratic susceptibility (lithium niobate) in the geometry where its highest component is involved. The incident radiation is tightly focused to further increase the efficiency. We consider two cases: the one where the beam waist is on the surface of the crystal and the one where it is in the bulk. We show that the first case is preferable due to a higher efficiency of SFG and due to the absence of Maker fringes [9] in the spectrum.

In our experiment, the input radiation is bright squeezed vacuum (BSV) generated through the high-gain parametric down-conversion (PDC). We demonstrate efficient broadband SFG on the surface of the crystal, revealing both the coherent peak, often interpreted as the result of the 'pump reconstruction', and the

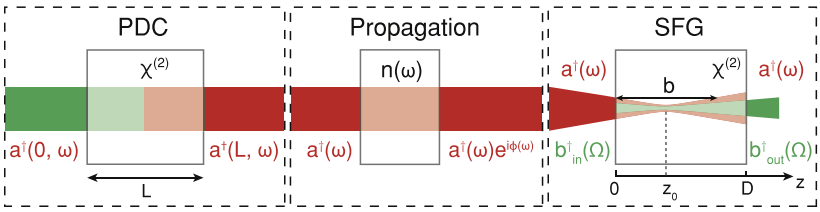

Figure 1. Schematic representation of SFG from BSV.

incoherent background [10, 11]. Since the SFG works as a fast coincidence circuit [12], we are able to extract from SFG spectra the number of frequency Schmidt modes, which in the case of low-gain PDC is equal to the degree of frequency entanglement of photon pairs [13]. Furthermore, we are able to observe broadband three- and four-frequency summation in the same geometry. For four-frequency summation, we also observe the 'coherent peak'. We describe these effects using Schmidt-mode formalism for PDC [14–16] and SFG with undepleted pump [17].

This paper is organized as follows. In section 2 we describe the theory for SFG from tightly focused PDC section 3 presents the experimental setup and section 4, the results. Section 5 concludes the paper.

2. Theory

In this section we present the theory of SFG from tightly focused broadband radiation. As a pump we use BSV generated through high-gain PDC [14]. Figure 1 shows schematically the three stages of the nonlinear interaction: generation of broadband BSV, its propagation in a dispersive medium, and SFG in a nonlinear crystal from a tightly focused beam. Further, we calculate the SFG spectrum by describing all three stages in a semi-analytical way.

2.1. SFG from a tightly focused pump

We describe the SFG using the theoretical approach of [17]. In the undepleted pump approximation, the output plane-wave annihilation operator for SFG at frequency Ω is

$$\hat{b}_{\rm out}(\Omega) = \hat{b}_{\rm in}(\Omega) + \int {\rm d}\omega\ K(\omega, \Omega)\, \hat{a}(\omega)\, \hat{a}(\Omega - \omega), \tag{1}$$

where $\hat{b}_{\rm in}$ is the input plane-wave annihilation operator and $\hat{a}(\omega)$ is the pump plane-wave annihilation operator. The transfer function $K(\omega, \Omega)$ for a plane-wave pump [17] is

$$\begin{aligned} K_{\rm pw}(\omega, \Omega) &= \beta(\omega, \Omega) \int_0^D {\rm d}z\ \exp(-{\rm i}\Delta\kappa(\omega, \Omega)z) \\ &= \beta(\omega, \Omega)\ D\ {\rm sinc}\left(\frac{\Delta\kappa(\omega, \Omega)D}{2}\right) \exp\left(\frac{-{\rm i}\Delta\kappa(\omega, \Omega)D}{2}\right), \end{aligned} \tag{2}$$

where $\beta(\omega, \Omega) \sim \chi^{(2)}\sqrt{\omega(\Omega - \omega)\Omega}$, $\chi^{(2)}$ is the quadratic susceptibility, $\Delta\kappa(\omega, \Omega) \equiv \kappa(\Omega) - \kappa(\omega) - \kappa(\Omega - \omega)$ is the wavevector mismatch for SFG, and D is the length of the SFG crystal. For simplicity we assume $\beta(\omega, \Omega) \equiv \beta$ is a constant.

In the case of a tightly focused pump the plane-wave approximation does not hold. In particular, the Gouy phase becomes important. To take it into account for SFG from a Gaussian beam, we insert the factor $(1 + 2{\rm i}(z - z_0)/b)^{-1}$ into the expression for the transfer function [18, 19],

$$K_{\rm G}(\omega, \Omega) = \beta \int_0^D {\rm d}z\ \frac{\exp(-{\rm i}\Delta\kappa(\omega, \Omega)z)}{1 + 2{\rm i}(z - z_0)/b}. \tag{3}$$

Here, $b = \kappa_0 w_0^2$, z_0, and w_0 are the confocal parameter, the waist position, and the radius of the pump beam, respectively, and $\kappa_0 = n(\omega_0)\omega_0/c$ is the wavevector at the degenerate frequency ω_0 (see figure 1). For simplicity, we assume that the pump beam parameters are the same for all frequencies. In the case of weak focusing, $b \gg D$, equation (3) simplifies to equation (2).

2.2. PDC radiation

In this paper the input radiation for SFG is multimode BSV generated through high-gain PDC. Following the approach of [15], we describe the PDC in terms of the averaged momentum operator. In the case of collinear

PDC along the z axis, it has the form

$$\hat{G}_{\rm int}(z) = \hbar\Gamma \iint {\rm d}\omega_{\rm i}\,{\rm d}\omega_s\; F(\omega_{\rm i},\,\omega_s)\hat{a}^{\dagger}(z,\,\omega_{\rm i})\hat{a}^{\dagger}(z,\,\omega_s) + {\rm h.c.}, \tag{4}$$

where Γ characterizes the interaction strength and s, i indices denote the signal and idler waves, respectively. The joint spectral amplitude (JSA) $F(\omega_i, \omega_s)$ for the PDC generated in a nonlinear crystal with the length L is [20],

$$F(\omega_i,\,\omega_s) = f_{\rm p}(\omega_i + \omega_s){\rm sinc}\left(\frac{\Delta k(\omega_i,\,\omega_s)L}{2}\right)\exp\left(\frac{{\rm i}\Delta k(\omega_i,\,\omega_s)L}{2}\right), \tag{5}$$

where $f_{\rm p}(\omega)$ is the pump spectral amplitude, $\Delta k(\omega_i,\,\omega_s) \equiv k_{\rm p}(\omega_i + \omega_s) - k_s(\omega_s) - k_i(\omega_i)$ is the phase mismatch. For the type-I phase matching, $k_{\rm p}(\omega_{\rm p}) = n_{\rm e}(\omega_{\rm p},\,\theta)\omega_{\rm p}/c$, $k_{s,i}(\omega_{s,i}) = n_{\rm o}(\omega_{s,i})\omega_{s,i}/c$, where $n_{\rm o}$ and $n_{\rm e}$ are ordinary and extraordinary refractive indices and θ is the optic axis angle w.r.t. $k_{\rm p}$.

The Heisenberg equation for the monochromatic-wave annihilation operators,

$$\frac{\partial\hat{a}(z,\,\omega)}{\partial z} = \frac{\rm i}{\hbar}[\hat{a}(z,\,\omega),\,\hat{G}_{\rm int}(z)], \tag{6}$$

can be analytically solved using the Schmidt decomposition of the JSA. The latter is symmetric for type-I phase matching, $F(\omega_i, \omega_s) = F(\omega_s, \omega_i)$, therefore

$$F(\omega_i,\,\omega_s) = \sum_n \sqrt{\lambda_n}\,\varphi_n(\omega_i)\,\varphi_n(\omega_s), \tag{7}$$

where the Schmidt modes $\{\varphi_n(\omega)\}$ form an orthonormal basis and the Schmidt eigenvalues λ_n are positive. Note that generally the JSA and $\varphi_n(\omega)$ are complex functions.

We introduce the Schmidt-mode creation and annihilation operators,

$$\begin{aligned}\hat{A}_n^{\dagger} &= \int {\rm d}\omega\;\varphi_n(\omega)\hat{a}^{\dagger}(0,\,\omega),\\ \hat{A}_n &= \int {\rm d}\omega\;\varphi_n^{*}(\omega)\hat{a}(0,\,\omega).\end{aligned} \tag{8}$$

They have standard commutation relations,

$$[\hat{A}_n,\,\hat{A}_m^{\dagger}] = \delta_{nm}, \quad [\hat{A}_n,\,\hat{A}_m] = 0. \tag{9}$$

Thus the solution of equation (6) is [14]

$$\hat{a}(L,\,\omega) = \hat{a}(0,\,\omega) + \sum_n \varphi_n(\omega)(S_n\hat{A}_n^{\dagger} + (C_n - 1)\hat{A}_n), \tag{10}$$

where $S_n = \sinh(\Gamma_n)$, $C_n = \cosh(\Gamma_n)$, and $\Gamma_n \equiv \Gamma\sqrt{\lambda_n}\,L$ is the parametric gain of the nth mode. Then the PDC spectral distribution of the photon number is

$$N_{\rm PDC}(\omega) = \langle 0|\hat{a}^{\dagger}(L,\,\omega)\hat{a}(L,\,\omega)|0\rangle = \sum_n S_n^2|\varphi_n(\omega)|^2. \tag{11}$$

The effective number of Schmidt modes K can be found as [14]

$$K = \left[\sum_n\left(\frac{S_n^2}{\sum_m S_m^2}\right)^2\right]^{-1}. \tag{12}$$

Here we find the Schmidt modes numerically using the Takagi factorization [21],

$$\mathscr{F} = \mathscr{U}\Sigma\mathscr{U}^{T}, \tag{13}$$

where $\mathscr{F}$ is a matrix corresponding to $F(\omega_i,\,\omega_s)$, $\mathscr{U}$ is a unitary matrix, and Σ is a diagonal matrix with the singular values $\sigma_n = \sqrt{\lambda_n}$. The discretized Schmidt modes $\varphi_n(\omega)$ are given by columns of matrix $\mathscr{U}$.

2.3. SFG from BSV

According to equation (1), the spectral distribution of the photon number in the sum frequency radiation is

$$\begin{aligned}N_{\rm SFG}(\Omega) = \langle 0|\hat{b}_{\rm out}^{\dagger}(\Omega)\hat{b}_{\rm out}(\Omega)|0\rangle &= \iint {\rm d}\omega_1{\rm d}\omega_2\\ &\times K^{*}(\omega_1,\,\Omega)K(\omega_2,\,\Omega)\langle 0|\hat{a}^{\dagger}(\omega_1)\hat{a}^{\dagger}(\Omega - \omega_1)\hat{a}(\omega_2)\hat{a}(\Omega - \omega_2)|0\rangle.\end{aligned} \tag{14}$$

We obtain

$$N_{\rm SFG}(\Omega) = \left|\sum_n C_nS_nI_{nn}(\Omega)\right|^2 + 2\sum_{n,m} S_n^2S_m^2\,|I_{nm}(\Omega)|^2, \tag{15}$$

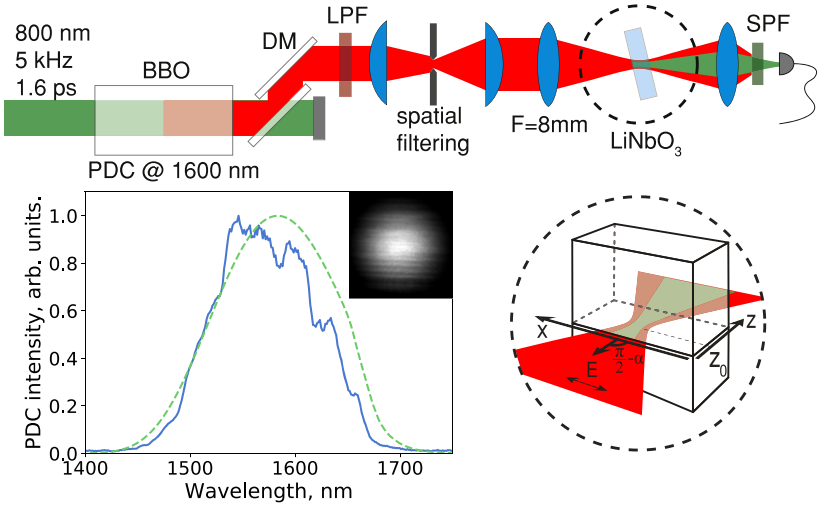

Figure 2. Top: experimental setup. Bottom left: measured (blue solid line) and calculated (green dashed line) PDC spectra and PDC beam after spatial filtering (inset). Bottom right: sketch of SFG under tight focusing.

where $I_{nm}(\Omega)$ is the inter-modal interaction integral,

$$I_{nm}(\Omega) = \int \mathrm{d}\omega\ K(\omega, \Omega)\varphi_n(\omega)\varphi_m(\Omega - \omega). \tag{16}$$

For a very thin crystal, $D \to 0$, $K(\omega, \Omega) \to$ const; then $I_{nm}(\Omega)$ is proportional to the convolution of the Schmidt modes.

In the presence of frequency-independent loss, or reduced efficiency of the SHG, the right-hand part of equation (16) will only acquire a constant factor smaller than the unity. This can be verified by describing loss with the help of a beamsplitter with constant transmission.

Expression (15) for the SFG spectrum contains two terms. The first one, so-called coherent contribution, corresponds to the SFG from each Schmidt mode with itself, i.e. the process reverse to PDC. It results in a narrow spectral peak with the width comparable to the one of the PDC pump. In the literature, the appearance of this peak is sometimes called 'the pump reconstruction' [11]. The second term, the incoherent contribution, is caused by the SFG from different (uncorrelated) Schmidt modes. It gives a pedestal with the width determined by the whole PDC spectrum. Note that expression (15) is valid for any parametric gain.

Previously the coherent and incoherent SFG contributions were obtained for a PDC with narrowband pump see, for instance [17, 22]. Our result (15) uses the Schmidt mode formalism that takes into account the finite width of photon correlations, which is significant for PDC generated by short pulses. In particular, it shows that the width of the 'coherent' peak is not the same as the one of the pump; it is somewhat broader (will be discussed later).

Note that here we considered the case where PDC has a single spatial mode. This approach is valid for waveguide PDC sources [23], for specially engineered PDC sources [24] and in the presence of spatial filtering (as in our experiment). In the general case, PDC is multi-mode both in time and in space, and one should take into account the overlap between PDC and SFG spatial modes.

2.4. Dispersion effects in SFG

In the course of propagation in a dielectric medium, a broadband radiation undergoes dispersion spreading. We take it into account through the replacement $\hat{a}^\dagger(L, \omega) \to \hat{a}^\dagger(L, \omega)\mathrm{e}^{\mathrm{i}\phi(\omega)}$, where $\phi(\omega)$ is the PDC nonlinear phase shift (chirp). This substitution leads to the replacement $\varphi_n(\omega) \to \varphi_n(\omega)\mathrm{e}^{\mathrm{i}\phi(\omega)}$ and $\varphi_m(\Omega - \omega) \to \varphi_m(\Omega - \omega)\mathrm{e}^{\mathrm{i}\phi(\Omega-\omega)}$ in equation (16).

3. Experimental setup

Our experimental setup is shown in figure 2 (top). PDC is produced in a 10 mm BBO crystal with type-I collinear and frequency degenerate phase matching [25]. The pump, propagating at ~19.9° w.r.t. the optic axis, is the radiation of an amplified Ti: Sapphire laser. It has the central wavelength 800 nm, the pulse duration 1.6 ps, the repetition rate 5 kHz and the mean power 3 W. To reduce the directional amplification caused by the spatial walk-off [26], the pump is focused into the crystal by means of a cylindrical lens with the 700 mm focal length.

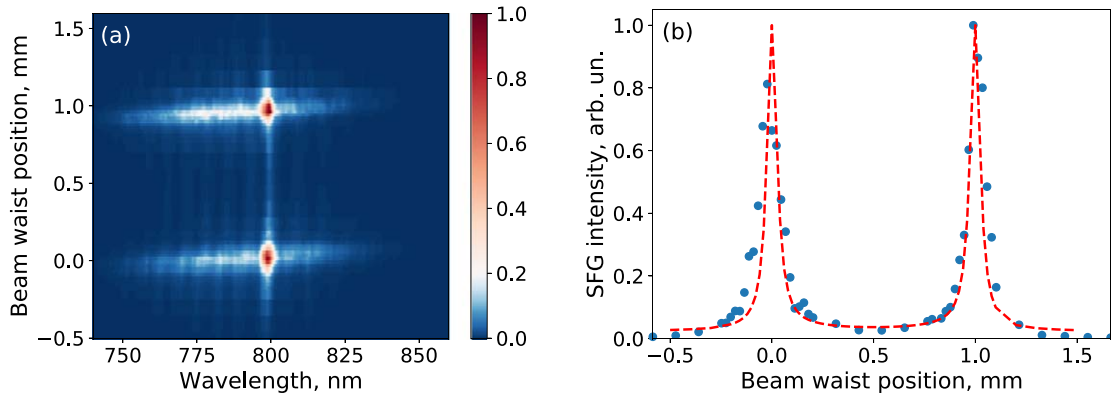

Figure 3. SFG spectrum (a) and SFG signal at 800 nm (b), measured (blue dots) and calculated (red line), versus the PDC beam waist position.

The pump remains unfocused and relatively broad (2.6 mm) in the horizontal direction. It is cut off by two dielectric dichroic mirrors and two longpass filters (LPF). Together they attenuate the pump by about 18 orders in magnitude and fully block the stray light at 800 nm.

Due to pump focusing, BSV is single-mode in the vertical direction. In the horizontal one we filter it to a single mode with a 140 μm vertical slit in the focal plane of a 200 mm lens. After filtering, the number of photons per pulse is about 10^{10}, which corresponds to about 6 μW of mean power. The beam is collimated by a 300 mm cylindrical lens thereafter; a Gaussian beam with an extremely broadband spectrum (FWHM of 140 nm) is formed. Figure 2 (bottom left) shows the beam (inset) and the spectrum, calculated (green line) and measured with an IR spectrometer (Hamamatsu-C11482GA, blue line). We measure the parametric gain $\Gamma_0 = 10.5$ for the first Schmidt mode. The small difference between experimental and numerical spectra is introduced by dielectric mirrors that are used in the experimental setup (not shown in figure 2).

The BSV beam is focused into a 1 mm $LiNbO_3$ crystal doped with 5.1% of Mg [27, 28] by means of an aspherical lens with the 8 mm focal length. Our focusing results in the beam waist $2w_0 \approx 6$ μm and the confocal parameter $b \approx 40$ μm. Tighter focusing is unappropriate due to chromatic aberrations of the lens, while softer focusing leads to more pronounced Maker fringes (see the next section). The $LiNbO_3$ crystal has its optical axis parallel to the facet, therefore the SFG occurs through the $ee \rightarrow e$ interaction without phase matching. The coherence length of this interaction, $\pi/\Delta\kappa$, is extremely small: about 4 times smaller than b. On the other hand, this interaction has very large quadratic susceptibility component $\chi^{(2)} = 2d_{33} \sim 60$ pm V^{-1}. In our measurements we tune the angle of incidence α and beam waist position z_0 w.r.t the crystal (figure 2, bottom right). The generated light is separated from BSV by shortpass filters (SPF) and measured with a visible spectrometer (Avantes AvaSpec-ULS3648) with 1.3 nm resolution.

4. Results and discussion

Figure 3(a) shows how the SFG spectrum depends on the beam waist position inside the crystal. The SFG intensity takes its highest values when BSV is focused on one of the crystal facets; focusing in the bulk leads to less efficient SFG.

Such behavior is caused by the Gouy phase for the SFG pump radiation and has nothing to do with so-called surface nonlinear susceptibility. The Gouy phase differs by π before and after the waist; therefore it leads to an additional phase shift in the nonlinear polarization. As a result, the SFG contributions before and after the waist interfere destructively, which leads to a low SFG intensity if the waist is in the bulk. Variation of the beam focusing or the crystal length strongly affects this behavior.

The theory from equations (3), (15) and (16) predicts the same effect. Theoretical SFG signal at 800 nm (figure 3(b), red line) agrees with the experimental one (blue dots). The latter is a 1D cross-section of figure 3(a).

The difference between the experimental and theoretical PDC spectra was assumed small; therefore in the calculation we used frequency independent Fresnel losses. In our setup we are not able to measure the group delay dispersion (GDD). Therefore we use it as a fitting parameter (see section 2.4). The best agreement between the theory and experiment is obtained for GDD ≈ 200 fs^2. Furthermore, in order to take into account that the detection happens in wavelength-angular space, not in frequency-wavevector one, the calculated SFG spectra are corrected by the factor λ^{-4} in accordance with [29, 30].

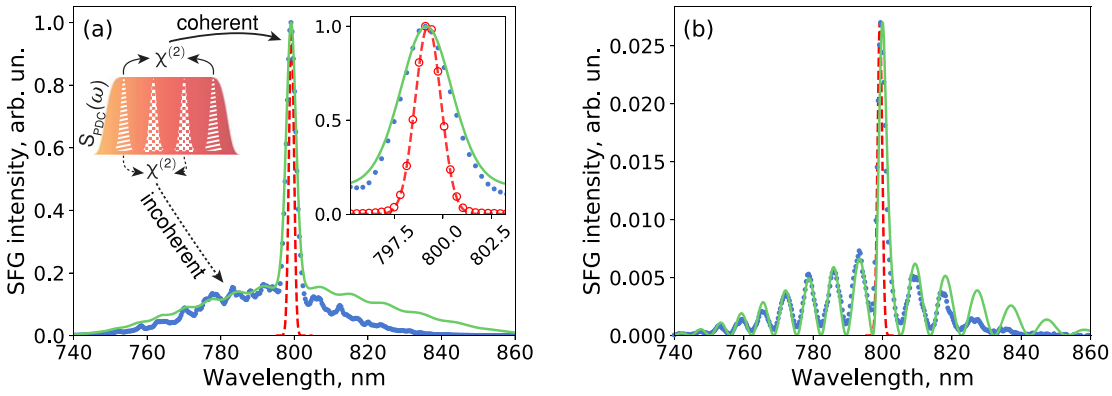

Figure 4. The experimental (blue dots) and theoretical (green line) SFG spectra for BSV focused (a) onto the facet and (b) into the bulk of the $LiNbO_3$ crystal. Red dashed line shows the spectrum of the Ti:Sapphire laser. The left inset in panel (a) schematically shows how the peak and the background are formed. The right inset in panel (a) is a zoom into the central part of the SFG spectrum. Red empty circles are the experimental points for the laser spectrum and the red dashed line is a Gaussian fit.

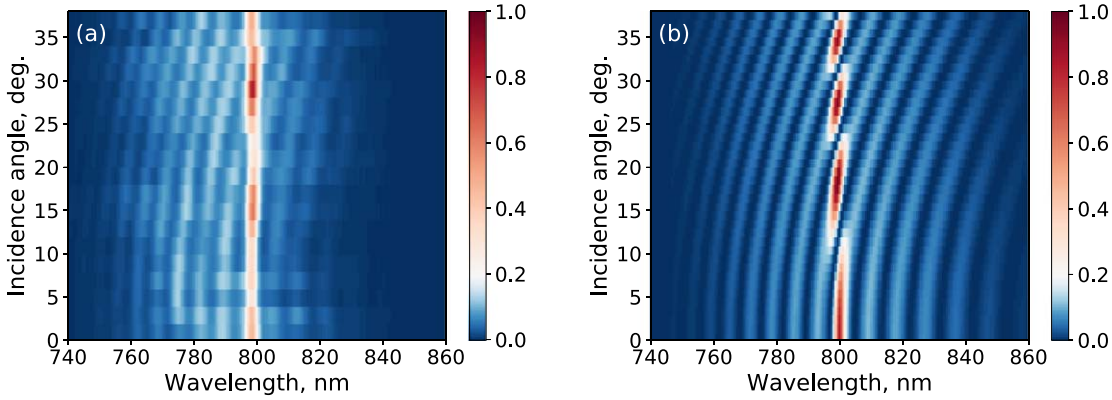

Figure 5. The experimental (a) and theoretical (b) SFG spectrum versus the angle of incidence α for the bulk focusing.

Both theoretical (blue dots) and experimental (green line) SFG spectra are shown in figure 4. Panel (a) shows the case of focusing onto the facet ($z_0 = 0$ mm) and panel (b), into the bulk ($z_0 = 0.5$ mm). The SFG spectrum contains two parts, the peak and the background. As discussed in section 2.3, the narrow peak corresponds to the coherent part and the broad background is incoherent one. In the bulk case, high-visibility fringes, similar to the Maker ones [9], appear due to the variation of the wavevector mismatch $\Delta\kappa$ with the wavelength. Their spectral positions depend on the angle of incidence α (figure 5); the theory predicts similar behavior. The fringe period scales as the inverse length of the crystal and depends on the SFG coherence length. For longer confocal parameters, the fringes become visible even under focusing onto the crystal facet.

Generally SFG can be interpreted as a fast correlator or coincidence circuit [12]. Expanding this analogy further, one can set the correspondence between the SFG spectrum and the spectral distribution of coincidences used to measure the joint spectral intensity (JSI) [31]. Then in the case of SFG from BSV, the width of the peak $\Delta\omega_{\mathrm{coh}}$ corresponds to the 'conditional width' of the JSI, which is the spectral distribution of the coincidence rate for a fixed frequency of the idler photon. Meanwhile, the width of the background $\Delta\,\omega_{\mathrm{incoh}}$ corresponds to the JSI 'unconditional width', which is the spectral width of the signal radiation. The ratio of the unconditional and conditional widths, according to [13], can be used to assess the degree of frequency entanglement for photon pairs, as it is close to the number of the Schmidt modes in the PDC spectrum. It follows that the ratio of the spectral widths, $R = \Delta\omega_{\mathrm{incoh}}/\Delta\omega_{\mathrm{coh}}$, can be also interpreted as the Schmidt number K.

To test this statement, we have calculated both the Schmidt number K, using equation (12), and the resulting ratio R for different values of the pump pulse duration. The result is shown in figure 6(a); as expected, we see that $R = K$. In experiment we get $R_{\mathrm{exp}} = 12.7$, which is smaller than the expected one $K_{\mathrm{theor}} = R_{\mathrm{theor}} = 19.5$, because the BSV spectrum is partially cut off due to experimental imperfections, and this leads to a reduced $\Delta\omega_{\mathrm{incoh}}$.

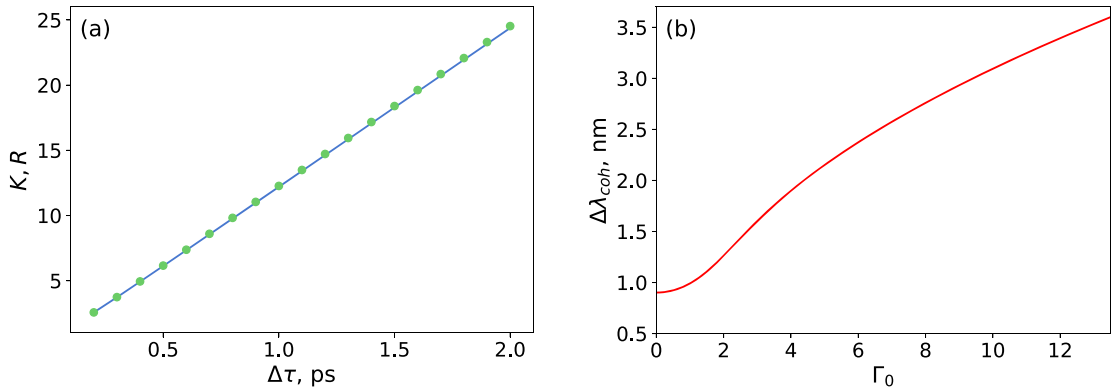

Figure 6. (a) The Schmidt number K (blue line) and the ratio R (green dots) calculated as functions of the PDC pump pulse duration. (b) The calculated spectral bandwidth of the peak $\Delta\lambda_{\mathrm{coh}}$ versus the parametric gain. At low gain, $\Gamma_0 \ll 1$, $\Delta\lambda_{\mathrm{coh}}$ is equal to the PDC pump bandwidth.

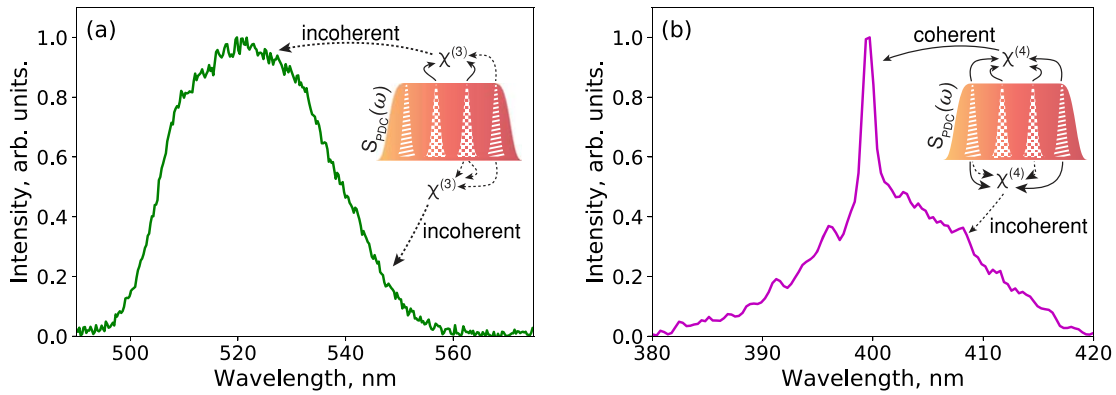

Figure 7. The three-frequency summation (a) and four-frequency summation (b) generated in the $LiNbO_3$. The PDC is focused in the facet of the crystal. The insets show the schemes for the corresponding frequency summation processes.

As mentioned above, frequency-independent losses do not affect the validity of this method. Meanwhile, if losses depend on the frequency or the transfer function $K(\omega, \Omega)$ is not broad enough, the result will change. This is why it is important to make SFG broadband by avoiding phase matching.

We see that both the experiment and the theory show the coherent peak broader than the PDC pump spectrum (figure 4(a), red dashed line). This effect was absent in the works where the number of Schmidt modes was very large due to the use of smaller pump bandwidths [10, 11]. It becomes noticeable for a finite number of Schmidt modes, especially with the increase of the parametric gain, which leads to an increase in the 'conditional width'. A similar increase of the 'conditional width' at high-gain PDC was observed in the frequency domain [30] and more precisely measured in the angular one [32]. Our theory gives the same result; the spectral bandwidth of the coherent peak increases with the increase in the parametric gain (figure 6(b)).

Non-phase-matched generation is also possible for higher-order nonlinear optical effects where it is usually difficult to satisfy the phase matching. Similarly to the SFG case considered above, strong focusing in the bulk can completely suppress high-order nonlinear optical processes [18, 19]. Focusing near the surface allows one to increase their efficiency as well.

To demonstrate it, we observe the three- and four-frequency summation of multimode PDC radiation near the surface of the same $LiNbO_3$ crystal. They occur through $eee \rightarrow e$ and $eeee \rightarrow e$ interactions, respectively. Figure 7 shows the measured spectra. Similarly to the case of SFG, for four-frequency summation we observe the coherent peak and the incoherent background, while for three-frequency summation there is no peak. This behavior, the even harmonics containing a peak and the odd ones, not, has been predicted theoretically for two-photon correlated light [33] but never observed in an optical experiment, to the best of our knowledge.

Qualitatively, this effect can be understood by considering that photons are produced in pairs: the coherent peak occurs if only both photons of a pair are involved into the process (see insets in figures 4(a) and 7). In other words, as for SFG, the peak corresponds to the frequency summation only from correlated photons, while the background, to all other possible combinations. For the four-frequency summation the coherent peak will be

produced from two photon pairs. In three-frequency summation, nonlinear interaction occurs between three BSV photons, so that one photon from the two pairs does not match to this process. This leads to the absence of a sharp peak in the frequency spectra of odd-order nonlinear processes. Moreover, the peak becomes less pronounced as the order of the harmonic increases, because the amount of combinations forming the background increases faster than the one forming the peak. A rigorous theoretical consideration for the case of delta-correlated two-photon light can be found in [33].

Previously, the coherent and incoherent contributions of PDC radiation were observed only for SFG and only under phase matching [7, 10, 11, 34]. Our results show that even without phase matching a pronounced narrowband coherent contribution and a broad incoherent contribution can be observed. Moreover, focusing near the surface of a nonlinear crystal suppresses the Maker fringes, which offers a possibility to use SFG as not just a broadband, but a *wavelength-independent* autocorrelator [35]. This type of autocorrelator will have an advantage over the one based on two-photon absorption (TPA) in semiconductors [36, 37]. Indeed, the operating wavelength of a TPA autocorrelator is limited for the wavelengths that satisfy the two-photon transition between the valence and conduction energy zones of a semiconductor band-gap. In the case of tightly focused non-phase matched SFG in the near-surface domain, the operating wavelength is only limited by the transparency window of the nonlinear crystal. Moreover, even in the presence of absorption at the sum frequency it is possible to measure the temporal characteristics of light [38].

5. Conclusion

We have shown that non-phase matched SFG in a strongly nonlinear crystal can be used to study the spectral properties of broadband light. In particular, with the radiation of high-gain PDC at the input, the SFG spectra show both the coherent contribution (a narrow peak) and the incoherent contribution (a broad background), which so far have been only observed for phase matched or quasi-phase matched SFG. By tightly focusing the radiation on the surface of the crystal instead of the bulk, one can strongly increase the efficiency of SFG; otherwise the Gouy phase leads to the destructive nonlinear interference. Moreover, by using the surface one gets rid of the Maker fringes, which modulate the spectrum in the case of bulk SFG.

Certainly, the efficiency of non-phasematched SFG is still lower than the one of phase-matched SFG. This requires the brightness of the incident light to be high enough. We easily detect SFG from picosecond pulses containing 10^{10} photons; the lowest flux for which the SFG can still be seen with the spectrometer is about 10^{9} photons per pulse. By using single-photon detectors one can further improve the sensitivity of the method by 2–3 orders of magnitude.

The obtained experimental results allow a simple interpretation within the Schmidt-mode formalism. In particular, we have found that the Schmidt number is equal to the ratio of the widths of the incoherent background and the coherent peak observed in the SFG spectra. This method of measuring the Schmidt number requires the presence of the coherent peak, which can be observed as long as the signal-idler correlation is not completely lost. In particular, the loss of this correlation can occur due to the group velocity dispersion, but one can prevent it with the dispersion-compensating methods. Frequency independent Fresnel losses, although breaking the purity of the BSV state, do not affect the validity of the measurement.

The same geometry, with tight focusing of the input radiation on the surface of the same crystal, allowed us to observe, in addition to SFG, the three- and four-frequency summation. As expected from the theory, for the four-frequency summation, the spectrum consists of a pronounced coherent peak and incoherent background, while the three-frequency summation does not manifest the peak.

We believe that under tight focusing, non-phase matched SFG and its higher-order analogs can be used for the characterization of nonclassical light sources and form the base for an ultrafast wavelength-independent autocorrelator.

Acknowledgments

We thank R Penjweini for helpful discussions. MVC and KYuS acknowledge the financial support of the joint DFG–RFBR (Deutsche Forschungsgemeinschaft—Russian Foundation for Basic Research) Project No. CH1591/2-1—16-52-12031 NNIOa. DAK acknowledge the financial support of Russian Foundation for Basic Research Project No. 18-32-00710 and German-Russian Interdisciplinary Science Center Project No. P-2016a-5, P-2017a-19, P-2018a-16.

ORCID iDs

Kirill Yu Spasibko https://orcid.org/0000-0001-6667-5084

References

[1] Armstrong J A 1967 *Appl. Phys. Lett.* **10** 16–8
[2] Kane D J and Trebino R 1993 *IEEE J. Quantum Electron.* **29** 571–9
[3] Iaconis C and Walmsley I A 1998 *Opt. Lett.* **23** 792–4
[4] Pe'er A, Dayan B, Friesem A A and Silberberg Y 2005 *Phys. Rev. Lett.* **94** 073601
[5] O'Donnell K A and U'Ren A B 2009 *Phys. Rev. Lett.* **103** 123602
[6] Sensarn S, Ali-Khan I, Yin G Y and Harris S E 2009 *Phys. Rev. Lett.* **102** 053602
[7] Jedrkiewicz O, Blanchet J L, Brambilla E, Di Trapani P and Gatti A 2012 *Phys. Rev. Lett.* **108** 253904
[8] Schwarz S, Bessire B, Stefanov A and Liang Y C 2016 *New J. Phys.* **18** 035001
[9] Maker P D, Terhune R W, Nisenoff M and Savage C M 1962 *Phys. Rev. Lett.* **8** 21–2
[10] Abram I, Raj R K, Oudar J L and Dolique G 1986 *Phys. Rev. Lett.* **57** 2516–9
[11] Jedrkiewicz O, Blanchet J L, Gatti A, Brambilla E and Trapani P D 2011 *Opt. Express* **19** 12903
[12] Sensarn S, Yin G Y and Harris S E 2010 *Phys. Rev. Lett.* **104** 253602
[13] Fedorov M V, Efremov M A, Volkov P A and Eberly J H 2006 *J. Phys. B: At. Mol. Opt. Phys.* **39** S467–83
[14] Sharapova P, Pérez A M, Tikhonova O V and Chekhova M V 2015 *Phys. Rev.* A **91** 043816
[15] Peřina J 2015 *Phys. Rev.* A **92** 013833
[16] Christ A, Brecht B, Mauerer W and Silberhorn C 2013 *New J. Phys.* **15** 053038
[17] Dayan B 2007 *Phys. Rev.* A **76** 043813
[18] Rostovtseva V V, Saltiel S M, Sukhorukov A P and Tunkin V G 1980 *Sov. J. Quantum Electron.* **10** 616–20
[19] Boyd R W 2008 *Nonlinear Optics* 3rd edn (Boston, MA: Academic)
[20] Kim Y H and Grice W P 2005 *Opt. Lett.* **30** 908
[21] Chebotarev A M and Teretenkov A E 2014 *Appl. Math. Comput.* **234** 380–4
[22] Brambilla E, Jedrkiewicz O, Lugiato L A and Gatti A 2012 *Phys. Rev.* A **85** 063834
[23] Eckstein A, Christ A, Mosley P J and Silberhorn C 2011 *Phys. Rev. Lett.* **106** 013603
[24] Pérez A M, Iskhakov T S, Sharapova P, Lemieux S, Tikhonova O V, Chekhova M V and Leuchs G 2014 *Opt. Lett.* **39** 2403
[25] Spasibko K Y, Kopylov D A, Murzina T V, Leuchs G and Chekhova M V 2016 *Opt. Lett.* **41** 2827
[26] Pérez A M, Spasibko K Y, Sharapova P R, Tikhonova O V, Leuchs G and Chekhova M V 2015 *Nat. Commun.* **6** 7707
[27] Kitaeva G K, Kuznetsov K A, Naumova I I and Penin A N 2000 *Quantum Electron.* **30** 726
[28] Spasibko K Y, Kopylov D A, Krutyanskiy V L, Murzina T V, Leuchs G and Chekhova M V 2017 *Phys. Rev. Lett.* **119** 223603
[29] Klyshko D 1988 *Photons and Nonlinear Optics* (New York: CRC Press)
[30] Spasibko K Y, Iskhakov T S and Chekhova M V 2012 *Opt. Express* **20** 7507
[31] Di Lorenzo Pires H, Monken C H and van Exter M P 2009 *Phys. Rev.* A **80** 022307
[32] Brida G, Meda A, Genovese M, Predazzi E and Ruo-Berchera I 2009 *J. Mod. Opt.* **56** 201–8
[33] Masalov A V 1991 *Opt. Spektr.* **70** 648–52
[34] Dayan B, Pe'er A, Friesem A A and Silberberg Y 2003 arXiv:quant-ph/0302038
[35] Chekhova M V, Germanskiy S, Horoshko D B, Kitaeva G K, Kolobov M I, Leuchs G, Phillips C R and Prudkovskii P A 2018 *Opt. Lett.* **43** 375
[36] Takagi Y, Imamura S, Kobayashi T and Yoshihara K 1992 *Opt. Lett.* **17** 658
[37] Boitier F, Godard A, Dubreuil N, Delaye P, Fabre C and Rosencher E 2011 *Nat. Commun.* **2** 425
[38] Kintzer E S and Rempel C 1987 *Appl. Phys.* B **42** 91–5